INTRODUCTION. We consider the regime $\delta_b \geq r \quad \Leftrightarrow \quad \varepsilon \leq \Delta^{2/3} \equiv \delta_p / R$, where $\delta_b \sim \varepsilon^{-1/2} q\rho$ is the standard banana orbit width, $\varepsilon \equiv r/R$, $q_0 \equiv q(0)$ and $\Delta \equiv 2q_0\rho / R$. In this regime, the banana-shaped orbit is distorted into a *potato*-shaped orbit with a characteristic width of the order of δ_p. For a 1 MeV Hydrogen ion and typical parameters of the JET Tokamak, $\delta_p \sim 0.3$ m is about one third of the plasma minor radius. A correct description of the high energy ion orbits is important to assess their effects on the energy balance and on MHD modes active in the central region of a Tokamak plasma (internal kinks, fishbones, TAE).

ORBIT EQUATION. The orbit equation for the particle guiding centres can be obtained from the invariance of the energy, $\mathcal{E} \equiv m\mathrm{v}^2/2$, magnetic moment, $\mu \equiv m\mathrm{v}_\perp^2/2B$, and toroidal canonical momentum in axisymmetric plasmas, $P_\varphi = (Ze/c)\psi - mR\mathrm{v}_\parallel B_\varphi / B$, where $\psi \geq 0$ is the poloidal flux function. We consider a standard low-β Tokamak equilibrium where the departure from concentric flux surfaces is of order ε. Neglecting higher order corrections, let us set $\mathrm{v}_\parallel = \pm \mathrm{v}_{\perp 0}(\lambda + \varepsilon\cos\vartheta)^{1/2}$, where $\mathrm{v}_{\perp 0} \equiv (2\mu B_0/m)^{1/2}$ and $\lambda \equiv (\mathcal{E}/\mu B_0) - 1$ are constants of the motion. We define $\psi_\varphi \equiv cP_\varphi / Ze$. The orbit equation can be written as

$$\mathrm{v}_\parallel / \mathrm{v}_{\perp 0} = \pm(\lambda + \varepsilon\cos\vartheta)^{1/2} = (Ze/mcR_0\mathrm{v}_{\perp 0})(\psi - \psi_\varphi). \tag{1}$$

Let us introduce the dimensionless variables $\hat{r} \equiv r/\delta_p$, $\hat{\lambda} \equiv (R/\delta_p)\lambda$, $\hat{\psi} \equiv (2q_0/B\delta_p^{\,2})\psi$, $\hat{\psi}_\varphi \equiv (2q_0/B\delta_p^{\,2})\psi_\varphi$, where the characteristic potato width

$$\delta_p \equiv (2q_0\mathrm{v}_{\perp 0}/\Omega_0 R_0)^{2/3} R_0 \tag{2}$$

is defined here as a constant of the motion. For the sake of analytic progress, we shall assume that the fast ions are confined near the magnetic axis in a region of low magnetic shear, i.e. $(d\ln q / d\ln r) << 1$ for $r \leq \delta_p$. In this case, we can approximate $\hat{\psi} \approx \hat{r}^2$. Then, the orbit equation can be cast in the more compact form:

$$\pm(\hat{\lambda} + \hat{r}\cos\vartheta)^{1/2} = \hat{r}^2 - \hat{\psi}_\varphi. \tag{3}$$

The potato range is defined by the inequalities

$$\hat{\psi}_\varphi \leq 1, \qquad \hat{\lambda} \leq 1. \tag{4}$$

ORBIT CLASSIFICATION. A classification of the orbit types can be obtained by studying the intersections of the orbits with the poloidal midplane. Squaring Eq. (9), we are led to consider the real non-negative roots of the quartic polynomial

$$F(\hat{r}) = \hat{\lambda} \pm \hat{r} - (\hat{r}^2 - \hat{\psi}_\varphi)^2, \tag{5}$$

where the plus sign corresponds to intersections on the low field side ($\vartheta = 0$) and the minus sign corresponds to intersections on the high field side ($\vartheta = \pi$). The total number of intersections can be either 0, 2 or 4, corresponding to 0, 1 or 2 orbits. Limiting orbits correspond to the tangency of the straight lines $g_\pm(\hat{r}) = \hat{\lambda} \pm \hat{r}$ with the quartic $f(\hat{r}) = (\hat{r}^2 - \hat{\psi}_\varphi)^2$. Thus, the loci of these orbits in the $(\hat{\lambda}, \hat{\psi}_\varphi)$ plane are obtained from the solution of the system

$$\begin{cases} F = 0 \\ \partial F/\partial \hat{r} = 0 \end{cases} \quad \Rightarrow \quad \begin{cases} \hat{\lambda} = \mp\hat{r} + 1/16\hat{r}^2 \\ \hat{\psi}_\varphi = \hat{r}^2 \mp 1/4\hat{r} \end{cases} \tag{6}$$

Eliminating $\hat{r}$, we obtain two curves in the $(\hat{\lambda}, \hat{\psi}_\varphi)$ plane (Fig. 1). The curve obtained choosing the minus sign, $\lambda_-(\hat{\psi}_\varphi)$, corresponds to the locus of the counter-passing stagnation orbits. No orbits exist below this curve. The curve obtained choosing the plus sign has a cusp at $\hat{r} = 1/2 \Rightarrow \hat{\lambda} = \hat{\psi}_\varphi = 3/4$. Thus we can identify two branches: the lower branch, $\lambda_{+,}(\hat{\psi}_\varphi)$ which corresponds to the locus of the pinch orbits, and the upper branch, $\lambda_{+,}(\hat{\psi}_\varphi)$, which corresponds to the locus of the co-passing stagnation orbits. The cusp itself corresponds to a triple zero of F, i.e. to a pinch orbit where the inner loop degenerates to a point. The two branches together form the boundary between the one-orbit and the two-orbit regions of Fig. 1. Transitional orbits correspond to values of $\hat{\lambda}$ and $\hat{\psi}_\varphi$ such that the

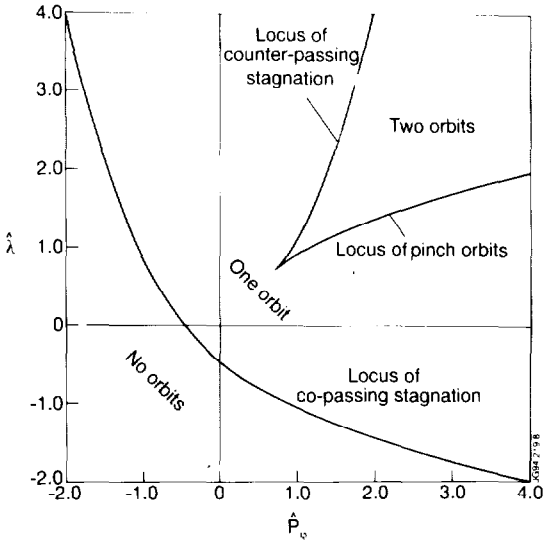

Figure 1

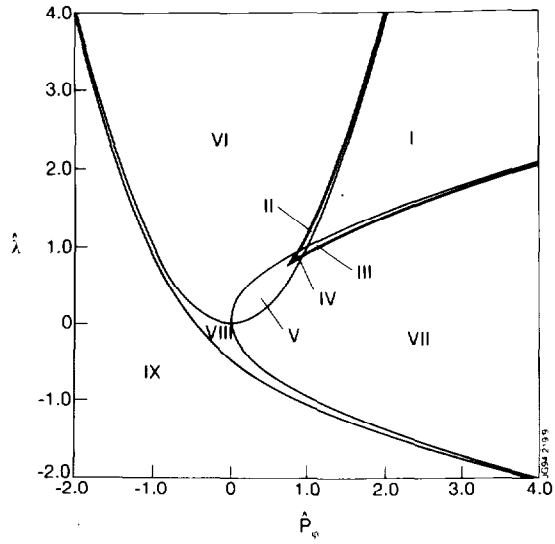

Figure 2

intersections between the curves $g_{\pm}(\hat{r})$ and $f(\hat{r})$ occur either at $\hat{r} = 0$ (orbits tangent to the axis) or at $\hat{r} = \hat{r}_{\varphi}$ (marginally trapped orbits). Thus we are led to consider the two additional parabolic curves $\hat{\lambda} = \hat{\psi}_{\varphi}^2$ (locus of the orbits that are tangent to the magnetic axis) and $\hat{\lambda} = (\hat{\psi}_{\varphi})^{1,2}$ for $\hat{\psi}_{\varphi} \geq 0$ (locus of the marginally trapped orbits). These two parabolas, in addition to the two curves of Fig. 1, give rise to eight regions in the $(\hat{\lambda}, \hat{\psi}_{\varphi})$ plane, corresponding to as many distinct topological orbit types, plus a ninth region where no orbits exist, as shown in Fig. 2. Limiting and transitional orbits can be found on the boundaries and corners among these regions. A complete orbit classification and representative examples are given in Table 1 and Figure 3.

TABLE 1: ORBITS IN REGIONS I-IX.

REGION	ORBITS	ORBIT TYPE(S)
I: $\hat{r}_{\varphi} < \hat{\lambda} < \hat{r}_{\varphi}^4$	two	-co-passing, encircling the axis -counter-passing, encircling the axis
II: $\max\{\hat{r}_{\varphi}, \hat{r}_{\varphi}^4\} < \hat{\lambda} < \hat{\lambda}_{+u}$	two	-co-passing, encircling the axis -counter-passing, high field side
III: $\hat{\lambda}_{+l} < \hat{\lambda} < \min\{\hat{r}_{\varphi}, \hat{r}_{\varphi}^4\}$	two	-mirror-trapped, encircling the axis -counter-passing, encircling the axis
IV: $\max\{\hat{\lambda}_{+l}, \hat{r}_{\varphi}^4\} < \hat{\lambda} < \min\{\hat{r}_{\varphi}, \hat{\lambda}_{+u}\}$	two	-mirror-trapped, encircling the axis -counter-passing, high field side
V: $\hat{r}_{\varphi}^4 < \hat{\lambda} < \hat{r}_{\varphi}$ – IV	one	-mirror-trapped, encircling the axis
VI: $\hat{\lambda} > \max\{\hat{\lambda}_{+u}, \hat{r}_{\varphi}, \hat{\psi}_{\varphi}^2\}$	one	-co-passing, encircling the axis
VII: $-\hat{r}_{\varphi} < \hat{\lambda} < \min\{\hat{r}_{\varphi}^4, \hat{\lambda}_{+l}\}$	one	-mirror-trapped, not encircling the axis
VIII: $\hat{\lambda}_{-} < \hat{\lambda} < \min\{\hat{\psi}_{\varphi}^2, \hat{r}_{\varphi}\}$	one	-co-passing, low field side
IX: $\hat{\lambda} < \hat{\lambda}_{-}$	no orbits	

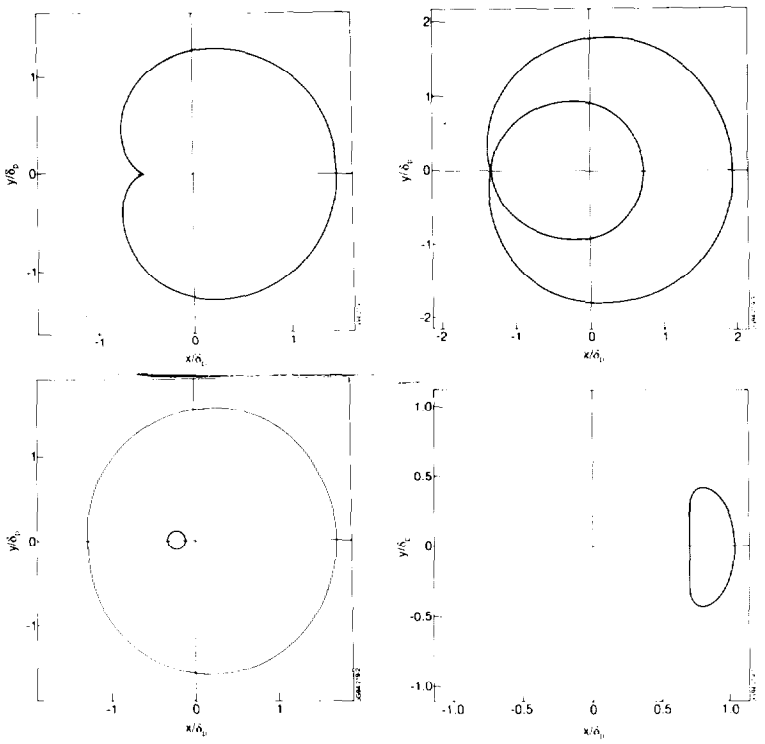

Fig. 3. Representative orbits: a) cusp orbit; b) pinch orbit; c) Pair of orbits in region II of Fig. 2, the inner orbit is close to the limiting counter-passing stagnation orbit; d) transitional orbit at the boundary between regions VII and VIII of Fig 2 (marginally trapped, not encircling the axis).

SLOWING-DOWN CHARACTERISTICS. In the high energy limit, only the collisional drag by the thermal electrons is important. The bounce-averaged Fokker-Plank equation for the fast ion distribution function, f_0, has the form

$$\frac{\partial f_0}{\partial t} = \left\langle \frac{1}{\tau_s} \right\rangle \frac{1}{v^2} \frac{\partial}{\partial v}\left(v^3 f_0\right) + \left\langle \frac{P_\varphi - Ze\psi/c}{\tau_s} \right\rangle \frac{\partial f_0}{\partial P_\varphi} + \langle S \rangle, \tag{7}$$

where angle brackets denote bounce averaging, τ_s is the slowing-down time and S is the fast ion source term. Using the variables $\hat{\psi}_\varphi, \hat{\lambda}$, assuming $\tau_s \approx$ const, and introducing the normalized time $\hat{t} \equiv t/\tau_s$, we obtain

$$\frac{dF}{d\hat{t}} = \frac{\partial F}{\partial \hat{t}} + \frac{2}{3}\hat{\lambda}\frac{\partial F}{\partial \hat{\lambda}} + \left[g(\hat{\psi}_\varphi, \hat{\lambda}; \sigma) + \frac{4}{3}\hat{\psi}_\varphi \right] \frac{\partial F}{\partial \hat{\psi}_\varphi} = \tau_s \langle S \rangle, \tag{8}$$

where $F \equiv v^3 f_0$ and the function $g(\hat{\psi}_\varphi, \hat{\lambda}; \sigma) \equiv \langle \hat{\psi} - \hat{\psi}_\varphi \rangle$, which is proportional to the fast ion toroidal

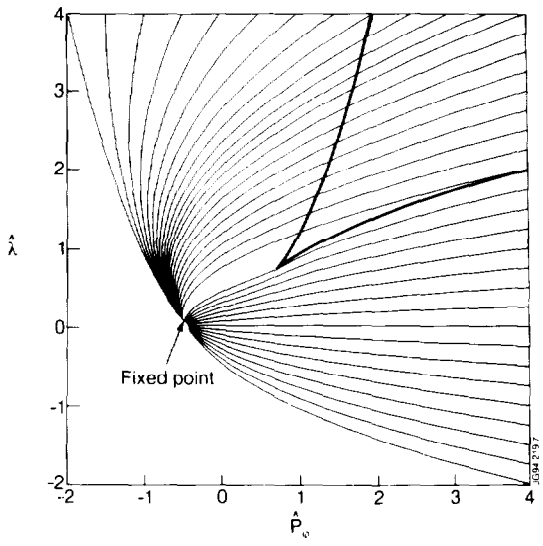

Figure 4

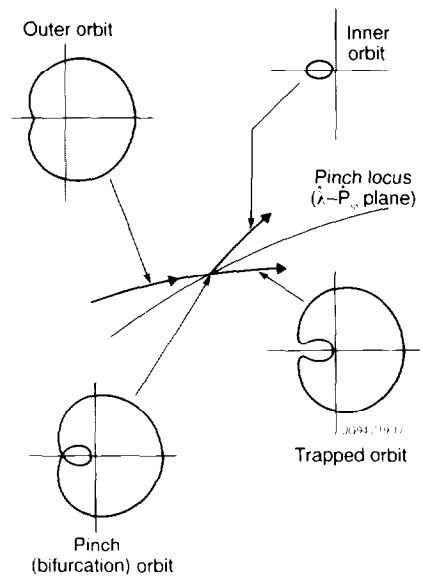

Figure 5

precession frequency, can be expressed in terms of elliptic integrals. The characteristic equations are

$$\frac{d\hat{\psi}_\varphi}{d\hat{t}} = g\left(\hat{\psi}_\varphi, \hat{\lambda}; \sigma\right) + \frac{4\hat{\psi}_\varphi}{3}, \qquad \frac{d\hat{\lambda}}{d\hat{t}} = \frac{2\hat{\lambda}}{3} \tag{9}$$

Analysis of this system reveals the existence of an unstable fixed point at

$$\hat{\lambda}_f = 0, \qquad \hat{\psi}_{\varphi f} = -3(16)^{-2/3} \approx -0.47 \tag{10}$$

The characteristic curves in the $(\hat{\lambda}, \hat{\psi}_\varphi)$ plane can be thought of as originating from this fixed point at $\hat{t} \to -\infty$, as shown in Fig. 4. Some of these curves intersect the pinch locus. At this time, a bifurcation occurs, as represented by the diagram of Fig. 5. Part of the orbits will become trapped (region VII of Fig. 2), while the remaining orbits will become counter-passing (regions I-III). The characteristic curves of the latter orbits are shown in Fig. 6. In order to assign a probability of transition to either of the two branches of the bifurcation diagram, the basins of attraction need to be studied.

The loci of co- and counter-passing stagnation orbits are mapped onto themselves during the slowing-down evolution. A significant inward radial transport has been found for those high energy ions that initially do not encircle the axis. An example is shown in Fig. 7a. Note that, as the particle loses energy, its orbit must eventually become a standard one. Therefore, particles that initially do not encircle the axis, either move onto the axis and then become a passing orbit, as in the case of Fig. 7a, or move a finite distance toward the axis and then become a standard banana orbit, as in the example of Fig. 7b.

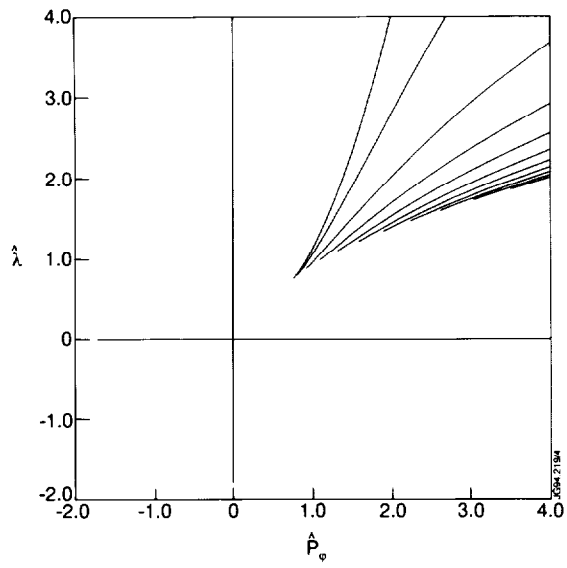

Figure 6

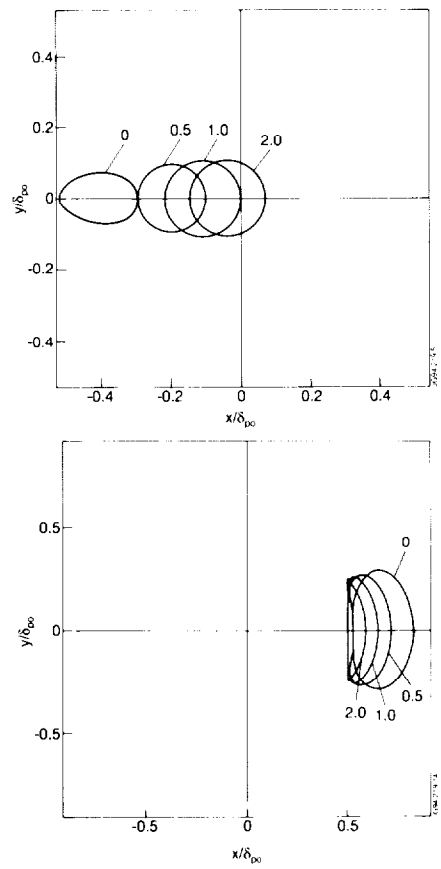

Figure 7

CONCLUSIONS. We have presented an analysis of nonstandard guiding centre orbits, which is relevant to MeV ions in a Tokamak. The orbit equation has been simplified from the start, so to enable us to present an analytic classification of the possible orbits. We have described the topological transitions of the orbits during collisional slowing down. In particular, the characteristic equations reveal the existence of a single fixed point in the relevant phase plane, and the presence of a bifurcation curve corresponding to the locus of the pinch orbits. A significant particle inward pinch has been discovered.